

Dalton Transactions

Accepted Manuscript



This is an *Accepted Manuscript*, which has been through the Royal Society of Chemistry peer review process and has been accepted for publication.

Accepted Manuscripts are published online shortly after acceptance, before technical editing, formatting and proof reading. Using this free service, authors can make their results available to the community, in citable form, before we publish the edited article. We will replace this *Accepted Manuscript* with the edited and formatted *Advance Article* as soon as it is available.

You can find more information about *Accepted Manuscripts* in the [Information for Authors](#).

Please note that technical editing may introduce minor changes to the text and/or graphics, which may alter content. The journal's standard [Terms & Conditions](#) and the [Ethical guidelines](#) still apply. In no event shall the Royal Society of Chemistry be held responsible for any errors or omissions in this *Accepted Manuscript* or any consequences arising from the use of any information it contains.

Cite this: DOI: 10.1039/c0xx00000x

www.rsc.org/xxxxxx

ARTICLE TYPE

[1,1- η^2 -dppe)-3-(NC₅H₅)-*closo*-1,2-RhSB₉H₈]: conformational lability and reactivity with H₂ upon protonation

Ana C. Mateo,^a Beatriz Calvo,^{a,b} Ramón Macías,^{*a} María José Artigas,^a Fernando J. Lahoz^a and Luis A. Oro^{*a,b}

Received (in XXX, XXX) Xth XXXXXXXXX 20XX, Accepted Xth XXXXXXXXX 20XX
DOI: 10.1039/b000000x

Metallaheteroboranes are versatile compounds that can be conveniently modified and eventually tailored by ligand modification at either the metal centre or the boron vertices. Recently, we have discovered that protonation of some rhodathiaboranes affords cationic clusters with interesting reaction chemistry. In order to tune the reactivity of some of these polyhedral boron-based compounds, we have prepared air-stable orange [1,1-(η^2 -dppe)-3-(NC₅H₅)-*closo*-1,2-RhSB₉H₈] (**2**) by the treatment of the known hydridorhodathiaborane [8,8,8-(H)(PPh₃)₂-9-(NC₅H₅)-*nido*-8,7-RhSB₉H₉] (**1**) with dppe. The new 11-vertex rhodathiaborane, **2**, reacts readily with triflic acid (TfOH) in CH₂Cl₂ to give orange cationic [8,8-(η^2 -dppe)-9-(NC₅H₅)-*nido*-8,7-RhSB₉H₉]⁺ (**3**). VT NMR experiments have allowed the characterization of a structural *closo*↔*nido* tautomerism, which involves hapticity changes in the ligation of the {SB₉H₉-(NC₅H₅)} moiety to the {Rh(dppe)} fragment, with the proton moving between the Rh(1)–B(3) and the B(9)–B(10) edges of the *closo*- and *nido*-isomers, respectively. The proton enhances the stereochemical non-rigidity and Lewis acidity of **3** versus the neutral **2**. This modification of the chemical and structural basis permits the efficient heterolytic splitting of the H–H bond, leading to the formation of new hydridorhodathiaborane isomers [8,8,8-(H)(η^2 -dppe)- μ -8,9-(H)-9-(NC₅H₅)-*nido*-8,7-RhSB₉H₁₀]⁺ (**4**) that are in equilibrium with the reactants, H₂ and **3**.

Introduction

The possibility to tune the reactivity of homogeneous catalysts by the modification of their chemical and structural basis by, for example, the use of different ligands is without doubt one of the reasons behind the interest in the organometallic chemistry of transition element complexes.¹

Just as metal complexes, the reactivity of metallaboranes and metallaheteroboranes can be adjusted by the systematic modification of the chemical composition of the metal-bound ligands as well as the heteroborane fragments.² There is thus large potential for the use of polyhedral boron-based clusters that incorporate different metal fragments in their structures (*i.e.*, metallaboranes and metallaheteroboranes) in areas such as catalysis.

In recent years, we have demonstrated this potential in that the reactivity of new 11-vertex rhodathiaboranes has been systematically tailored by changing the *exo*-polyhedral ligands at the rhodium centre, at a boron vertex or both.^{3–6} It has, thus, been possible to activate dihydrogen on the new 11-vertex *closo*-rhodathiaboranes, and to prepare hydridorhodathiaboranes capable of undergoing oxidative addition of *sp* C–H bonds, and catalytic hydrogenation and isomerization of olefins.^{7–9}

Most recently, we have discovered that protonation of some of these 11-vertex rhodathiaboranes with strong Brønsted acids is

a simple way of influencing the structural and electronic properties of these polyhedral clusters. By simple protonation, it is possible to labilize the metal-thiaborane linkage leading to an increase of the structural non-rigidity of the deltahedral clusters and of their Lewis acidity, promoting consequently new reactivity that has allowed the optimization of the H₂ splitting on cationic 11-vertex rhodathiaboranes.^{10, 11–14}

In this manuscript, the possibility of influencing the reactivity of metallaheteroboranes by modifying the *exo*-polyhedral ligands and by the protonation of the clusters is further demonstrated with the synthesis of new 11-vertex rhodathiaboranes that contain the *bis*-(diphenylphosphino)ethane (dppe) ligand. In comparison with monodentate phosphines previously studied,^{11, 13, 14} the use of a chelating ligand such as dppe has shown to have a large influence in the structural and electronic properties of the 11-vertex cluster, which has allowed (*i*) the characterization of a new tautomeric processes that reflects the non-rigidity of the dppe-ligated cationic species and (*ii*) the reversible addition of H₂ to the cage.

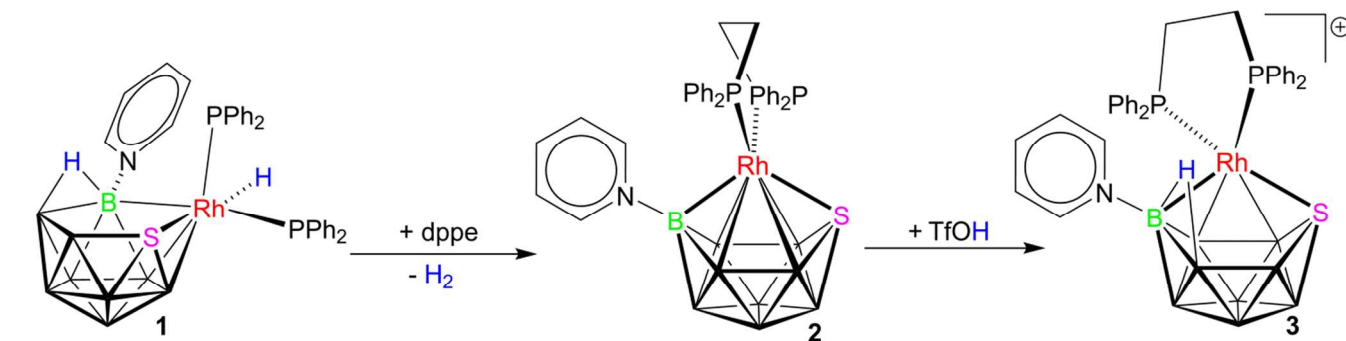
Results and discussion

Synthesis and characterization

The reaction of [8,8,8-(H)(PPh₃)₂-9-(NC₅H₅)-*nido*-8,7-RhSB₉H₉] (**1**) with dppe at the reflux temperature in dichloromethane affords the new dppe-ligated 11-vertex rhodathiaborane, [1,1-(η^2 -dppe)-3-(NC₅H₅)-*closo*-1,2-RhSB₉H₈] (**2**) with a 65% yield (Scheme 1).

The reaction involves the substitution of the two PPh₃ ligands by the chelating dppe ligand and the formal loss of H₂ from the cluster. From the cluster view point, the loss of two hydrogen atoms leads to the reduction of two skeletal electrons in the bonding of the cage, therefore, the observed *nido-to-closo*

structural transformation of the 11-vertex cluster is in accord with the electron counting rules derived by Wade.¹⁵ In other words, the reaction of **1** with dppe to give **2** is a ligand substitution and cluster oxidation process (Scheme 1).



Scheme 1 Reaction of **1** with dppe to give **2**, and its protonation with triflic acid to form **3**.

The treatment of **2** with triflic acid (TfOH) leads to the protonation of the *closo*-cage to give the polyhedral cation, [8,8-(η^2 -dppe)-9-(NC₅H₅)-*nido*-8,7-RhSB₉H₉]⁺ (**3**) (Scheme 1).

Compounds **2** and **3** have been characterized by multinuclear NMR spectroscopy, mass spectrometry and X-ray diffraction, and their structures and spectroscopic data are discussed below.

Table 1 lists some selected distances and angles of **2** and **3**. The molecular structure of **2** is based on an octadecahedron, which is the deltahedron that is predicted by simple application of the Wade rules for an 11-vertex *closo*-cluster with twelve skeletal

electron pairs. Alternatively, **2** can be described as a coordination compound that features an hexahapto ligation of the {SB₉H₈(NC₅H₅)} moiety to the rhodium atom.

The dimensions of the dppe-ligated cluster, **2**, are similar to those found for the *bis*-PMe₂Ph-ligated counterpart, [1,1-(PMe₂Ph)₂-3-(NC₅H₅)-*closo*-1,2-RhSB₉H₈].⁵ As expected, the Rh–P distances in the chelate are significantly shorter than in the derivative with monodentate phosphines. The structural effect of the chelating ligand is also manifest in the smaller P(1)–Rh(1)–P(2) angle [85.015(19) vs. 96.27(4)].

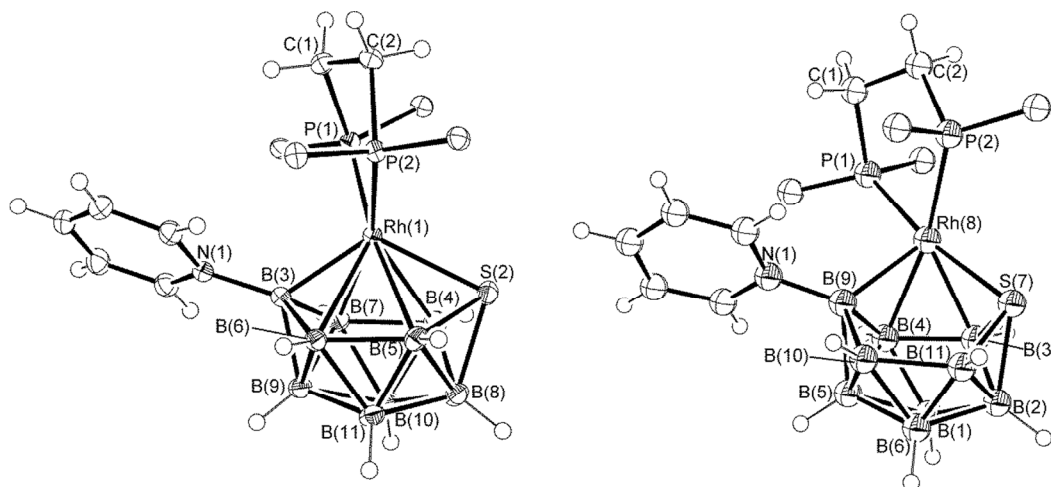


Fig. 1 ORTEP-type of drawing of [1,1-(η^2 -dppe)-3-(NC₅H₅)-*closo*-1,2-RhSB₉H₈] (**2**) and [8,8-(η^2 -dppe)-9-(NC₅H₅)-*nido*-8,7-RhSB₉H₉]⁺ (**3**).

Ellipsoids are shown at 50 % probability levels. The hydrogen atom along the B(9)–B(10) edge could not be found.

The molecular structure of the cationic cluster **3** was obtained from weakly diffracting slightly twinned crystal sample. In addition, disorder was found involving triflate anions and solvent molecules. The twin nature of the crystal and the crystallographic disorder precluded a precise analysis, notwithstanding the data allowed the unambiguous characterization of the polyhedral cation in the crystal (see experimental section and ESI for more details).

The cluster exhibits an 11-vertex *nido*-cluster geometry with

a five-membered {RhSB₃} open face (Figure 1). This structural attribute is manifest by the Rh(8)···B(10) and Rh(8)···B(11) non-bonding distances of 3.333(11) and 3.463(12) Å, respectively, which in compound **2** correspond to the Rh(1)–B(6) and Rh(1)–B(5) bonding lengths of 2.380(2) and 2.498(2) Å. A common feature of this type of 11-vertex *nido*-cages is that the {M(L)₂} units are twisted away from a reference plane through {M(8)B(1)B(6)}.⁴ In **3**, the dihedral angles Φ between the plane formed by {P(1)Rh(8)P(2)} and the {S(7)Rh(8)B(9)} plane is 63°, resembling the angles found in other *bis*-L₂-ligated *nido*-

metallaheteroboranes.⁴

The angle between the $\{S(7)Rh(8)B(9)\}$ and $\{S(7)B(2)B(5)B(9)\}$ planes, θ , is appropriate to examine for intermediacy of structure between conventionally *nido* compounds and *closo*-cages.⁴ This angle is virtually zero in 11-vertex octadecahedral clusters such as compound **2**, and in compound **3**, the angle is 45° , close to the value of 48° , found in its isoelectronic neutral counterpart $[8,8-(\eta^2\text{-dppp})\text{-nido-}8,7\text{-RhSB}_9\text{H}_{10}]$, which has been structurally well characterized by X-ray diffraction analysis.¹⁶

It is interesting to note that according to Wade rules compounds **2** and **3** contain 12 of skeletal electron pairs (sep), and both clusters are expected to exhibit an eleven-vertex *closo*-structure based on an octadecahedral geometry.¹⁵ Therefore, the structure of compound **3** is an example of an 11-vertex cluster that adopts a more open structure. It has been noted before that a discrepancy between the electron-counting rules and the structure is common among polyhedral molecules that incorporate C_{2v} fragments such as RhL_2 or PtL_2 .^{17, 18} In this regard, the rhodathiaborane $[8,8-(PPh_3)_2\text{-nido-}8,7\text{-RhSB}_9\text{H}_{10}]$ (precursor of **1**, and hence of **2** and **3**) has the same number of sep than **2** and **3** but its structure is that of an eleven-vertex cluster derived from and icosahedron by the removal of a vertex.^{19, 20}

The open *nido*-structures found in the neutral rhodathiaborane, $[8,8-(PPh_3)_2\text{-}8,7\text{-RhSB}_9\text{H}_{10}]$, and in the cationic pyridine adduct **3** arise by stabilization effects of the B–H–B bridging hydrogen atom on the pentagonal open face of both clusters (*vide infra*, Figure 4), with concomitant preference of *pseudo*-square-planar $\{Rh(L)_2\}$ centres for sixteen-electron configurations rather than eighteen-electron configurations.

The $^{11}B\text{-}\{^1H\}$ NMR spectrum of the *closo*-rhodathiaborane, **2**, shows six peaks in a 1:1:2:1:2:2 relative intensity ratio in the range $\delta(^{11}B)$ +53 to -35, which is in accord with a cluster of C_s -symmetry in solution. The pattern resembles readily the spectra of the previously reported, $[1,1-(PR_3)_2\text{-}3-(NC_5H_5)\text{-}closo\text{-}1,2\text{-RhSB}_9H_8]$, where $PR_3 = PPh_3; PMe_2Ph; PMe_3; PPh_3$ and PMe_3 ; or PPh_3 and PMe_2Ph (Figure 2).⁵ The highest frequency resonance corresponds to the pyridine-substituted B(3) vertex, being diagnostic of this type of polyhedral boron-based cluster. Figure 2 illustrates the remarkable similarity of the ^{11}B spectra among this series of eleven-vertex *closo*-rhodathiaboranes, suggesting that the change of the phosphine ligands at the rhodium centre does not alter significantly the overall shielding pattern of the boron nuclei. This trend could be viewed as the consequence of the cluster bonding network acting as an electron buffer capable of delocalising any excess of electron density at the metal centre. Thus, in principle, we could hypothesize that the alteration of the *exo*-polyhedral ligands at the rhodium centre does not have a large effect in the reactivity of the clusters, but this hypothesis is far to be true (*vide infra*). The $^{31}P\text{-}\{^1H\}$ spectrum of **2** shows a doublet at $\delta(^{31}P)$ +64.7, which confirms the presence of the dppe ligand bound to the rhodium atom, and the C_s -point symmetry of the cluster in solution.

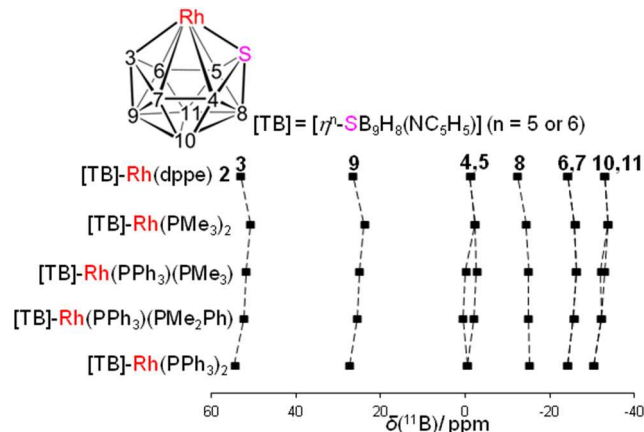


Fig. 2 ^{11}B NMR spectra representation of **2** and of $\{Rh(PR_3)_2\}$ bis-ligated analogues, $[1,1-(PR_3)_2\text{-}3-(NC_5H_5)\text{-}closo\text{-}1,2\text{-RhSB}_9H_8]$. Hatched lines connect equivalent positions.

The $^{11}B\{^1H\}$ NMR spectrum of the cationic cluster **3** shows four peaks in the interval $\delta(^{11}B)$ +40 to -23 with a 1:1:2:5 relative intensity ratio. This pattern implies a significant change with respect to the spectrum of the neutral reagent, **2**. Thus, upon protonation the resonance of the pyridine-substituted boron atom shifts 15 ppm towards lower frequencies; whereas the other signals approach to each other and overlay (see Figure S1). It is important to note that in the case of the previously reported analogues, $[1,1-(PR_3)_2\text{-}3-(NC_5H_5)\text{-}closo\text{-}1,2\text{-RhSB}_9H_8]$,⁵ where $PR_3 = PMePh_2, PPh_3$ and PMe_2Ph ; or PMe_3 and PPh_3 , the $^{11}B\text{-}\{^1H\}$ spectra of the protonated clusters exhibit the same pattern than the neutral parent clusters, suffering only a small deshielding.

The ^{11}B NMR data, therefore, suggest that compound **2** undergoes a significant structural and electronic change upon protonation to give **3**. This is confirmed by the analysis of the $^1H\text{-}\{^{11}B\}$ spectrum that shows a broad singlet at $\delta(^1H)$ -3.35 that can be assigned to a B–H–B bridging hydrogen atom, being diagnostic of a *closo*-to-*nido* structural change (Scheme 1, Figure S2). Once again, this differs significantly from the reactivity found in the *bis*- PR_3 -ligated *closo*-clusters, indicated above, which undergo selective protonation at the Rh(1)–B(3) edge, maintaining in solution the overall 11-vertex structure based on an octadecahedron.

An eleven-vertex *nido*-structure for **3** such as that depicted in Scheme 1 implies two ^{31}P nuclei with different chemical shifts, however, the $^{31}P\text{-}\{^1H\}$ NMR spectrum at room temperature exhibits a doublet at $\delta(^{31}P)$ +54.6. This suggests that the cationic rhodathiaborane, **3**, is stereochemically non-rigid undergoing intramolecular rearrangements that make equivalent the phosphorous-31 nuclei on the NMR time-scale.

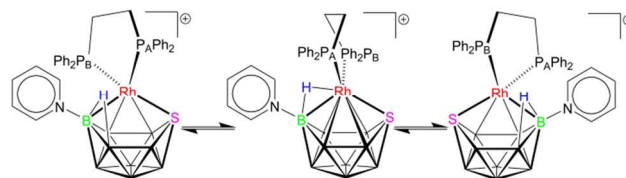
We should point out the lower value of the J_{RhP} coupling constant in **3** (118 Hz) compared with that of **2** (150 Hz), which suggests that protonation of the cage results in a marked different metal-to-thiaborane bonding interaction. A similar decrease in the J_{RhP} coupling constant was found upon protonation of $[1,1-(PR_3)_2\text{-}3-(NC_5H_5)\text{-}closo\text{-}1,2\text{-RhSB}_9H_8]$, where $PR_3 = PMePh_2, PPh_3$ and PMe_2Ph , or PMe_3 and PPh_3 , to give the corresponding cationic species, $[1,1-(PR_3)_2\text{-}3-(NC_5H_5)\text{-}closo\text{-}1,2\text{-RhSB}_9H_9]^+$.¹¹

Variable Temperature (VT) NMR studies. NMR studies at low temperatures have allowed us to propose that compound **3**

undergoes a rapid and reversible process of isomerisation in solution. Thus, the doublet in the $^{31}\text{P}\{-^1\text{H}\}$ NMR spectrum at room temperature broadens and shifts towards higher frequencies as the temperature decreases. Then, the very broad resonance splits into three signals (Figure 3). At 183 K, the spectrum exhibits a broad doublet at $\delta(^{31}\text{P}) +46.3$ and two overlapping doublets at $\delta(^{31}\text{P}) +57.4$ and $+58.0$.

This VT NMR behaviour is further illustrated in the corresponding $^1\text{H}\{-^{11}\text{B}\}$ NMR spectra that reveal how the low frequency singlet at -3.35 ppm broadens significantly when the temperature decreases from 300 to 243 K (Figure 3). Similar to the $^{31}\text{P}\{-^1\text{H}\}$ NMR spectrum, a more significant change occurs when the temperature is decreased further, and the B–H–B bridging proton resonance shifts 4 ppm towards lower frequencies at 183 K. The resulting very broad proton resonance at $\delta(^1\text{H}) -7.12$ is reminiscent of the low frequency multiplets found in the $^1\text{H}\{-^{11}\text{B}\}$ spectra of the 11-vertex cationic species $[1,1-(\text{PR}_3)_2-1,3-\mu(\text{H})-3-(\text{NC}_5\text{H}_5)\text{-}closo\text{-}1,2\text{-RhSB}_9\text{H}_8]^+$, where $\text{PR}_3 = \text{PMePh}_2$; PPh_3 and PMe_2Ph ; or PMe_3 and PPh_3 , which correspond to protons along the Rh(1)–B(3) edges of these octadecahedral *closo*-clusters.¹¹

Although in this case we do not observe neither $^1J_{\text{RhH}}$ or $^2J_{\text{PH}}$ coupling constants (probably due to the broadness of the peak), the low frequency proton resonance that results upon cooling **3** at 183 K can be assigned with good level of confidence to a bridging hydrogen atom along a Rh–B edge.



Scheme 2 Interconversion of *nido*- and *closo*-rhodathiaborane cations

Based on the VT NMR spectroscopic behaviour of **3**, we propose that this cationic species undergoes the rapid and reversible conversion of the *nido* rhodathiaborane cation to its *closo*-tautomer (Scheme 2). At higher temperatures, the major isomer is the *nido*-cluster featuring a pentagonal face on which the proton stays most probably along the B(9)–B(10) edge. At lower temperatures, the equilibrium shifts towards the formation of the *closo*-tautomer in which the proton occupies most likely a position along the Rh(1)–B(3) edge. The high mobility of this protic hydrogen atom and the consequent non-rigidity of the rhodathiaborane cluster do not allow the resolution of any coupling with either the rhodium or the phosphorous nuclei.

This prototypic *nido*–*closo* tautomerism can be described as the shift and half-rotation of the $\{\text{Rh}(\text{dppe})\}$ vertex above the six-membered face $\{\text{S}(7)\text{B}(3)\text{B}(4)\text{B}(9)\text{B}(10)\text{B}(11)\}$ of the thiaborane moiety in the *nido*-cluster. As the metal centre moves from a tetrahapto ligation with the $\{\text{SB}_9\text{H}_8(\text{NC}_5\text{H}_5)\}$ fragment in the *nido*-isomer to an hexahapto ligation in the *closo*-tautomer, there is a reverse shift of the bridging hydrogen atom from the B(9)–B(10) edge to the Rh(1)–B(3) edge. The exchange of the two phosphorous nuclei, demonstrated by NMR spectroscopy, implies the *pseudo*-rotation of the $\{\text{Rh}(\text{dppe})\}$ group that is performed via the *closo*-isomer. The two enantiomers of the *nido*-isomer interconvert in the course of this dynamic process (Scheme 2).

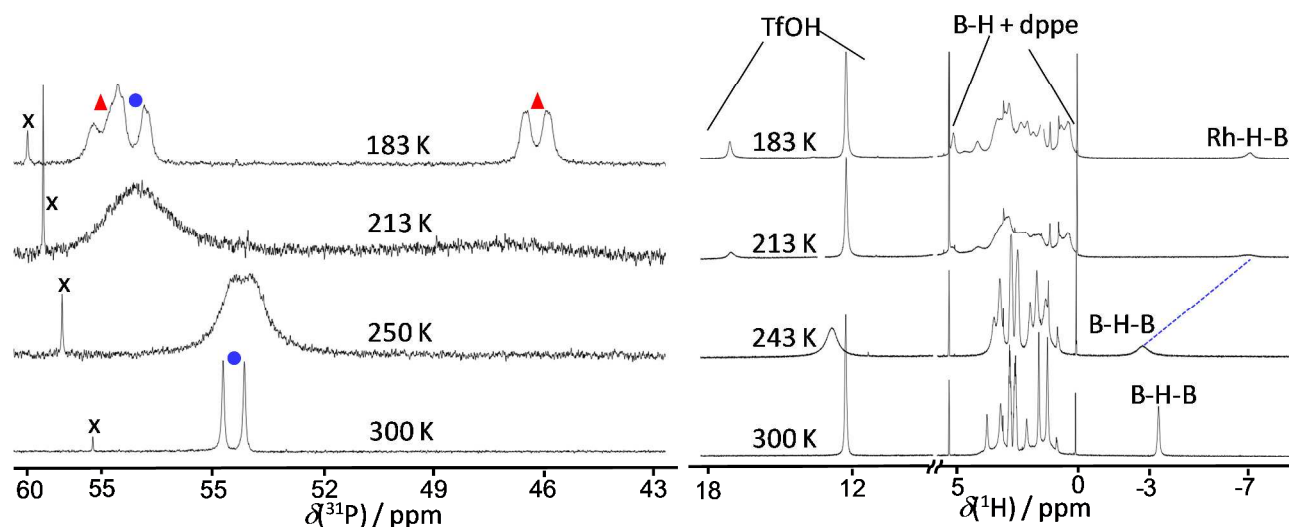


Fig. 3 Variable temperature (VT) $^{31}\text{P}\{-^1\text{H}\}$ (left) and $^1\text{H}\{-^{11}\text{B}\}$ (right) NMR spectra of **3**. The peaks marked with a red triangle in the VT $^{31}\text{P}\{-^1\text{H}\}$ correspond to the *nido*-isomer, and the overlapping peak marked with a blue circle is assigned to the *closo*-tautomer. The peak marked X is due to an impurity

60

Table 1. Selected interatomic distances (Å) and angles (°) for [1,1-(η^2 -dppe)-3-(NC₅H₅)-*closo*-1,2-RhSB₉H₈] (2) and [8,8-(η^2 -dppe)-9-(NC₅H₅)-*nido*-8,7-RhSB₉H₉]⁺ (3).

2		3	
Rh(1)–P(1)	2.2482(5)	Rh(8)–P(1)	2.274(3)
Rh(1)–P(2)	2.2748(5)	Rh(8)–P(2)	2.347(3)
Rh(1)–S(2)	2.3765(5)	Rh(8)–S(7)	2.392(3)
Rh(1)–B(3)	2.078(2)	Rh(8)–B(9)	2.159(10)
Rh(1)–B(4)	2.410(2)	Rh(8)–B(3)	2.238(12)
Rh(1)–B(5)	2.498(2)	Rh(8)⋯B(11)	3.463(12)
Rh(1)–B(6)	2.380(2)	Rh(8)⋯B(10)	3.333(11)
Rh(1)–B(7)	2.405(2)	Rh(8)–B(4)	2.249(10)
B(5)–B(8) _{longest}	1.916(7)	B(2)–B(3) _{longest}	1.883(17)
B(3)–B(7) _{shortest}	1.712(6)	B(6)–B(10) _{shortest}	1.748(16)
P(1)–Rh(1)–P(2)	85.015(19)	P(1)–Rh(8)–P(2)	82.96(9)
S(2)–Rh(1)–B(3)	119.68(6)	S(7)–Rh(8)–B(9)	93.3(3)
N(1)–B(3)–Rh(1)	128.28(14)	N(1)–B(9)–Rh(8)	122.3(7)
S(2)–Rh(1)–P(1)	123.234(19)	S(7)–Rh(8)–P(1)	168.85(9)
S(2)–Rh(1)–P(2)	103.954(19)	S(7)–Rh(8)–P(2)	94.30(9)

To facilitate the discussion below, it is convenient to bear in mind that the thiaborane fragment in these 11-vertex rhodathiaboranes forms donor-acceptor complexes or coordination compounds in which the {SB₉H₉(C₅H₅)} moiety is acting as a ligand with different degrees of hapticity.

In previous works, we demonstrated that the cationic *bis*-PR₃-ligated species, [(PMe₃)(PPh₃)(NC₅H₅)RhSB₉H₉]⁺, features a labile polyhaptic ligation of the {SB₉H₉(NC₅H₅)} moiety to the rhodium centre. This was determined in the solid state by the characterization of three different {Rh(PPh₃)(PMe₃)}-to- $\{\eta^n$ -SB₉H₉(NC₅H₅)} (n = 4 or 5) conformers in the unit cell: an uncommon case of conformational isomerism.

The new dppe-ligated polyhedral cation, **3**, features a more labile ligation of the thiaborane moiety to the {Rh(dppe)} vertex that results in a reversible *nido*↔*closo* isomerisation. This dynamic behaviour implies rapid hapticity changes in the {Rh(dppe)}-to- $\{\eta^n$ -SB₉H₈(NC₅H₅)} linkage from η^6 in the *closo* isomer to η^4 in the *nido*-cluster, which is the structure determined in the solid state by X-ray crystallography (Figure 1).

The stereochemical non-rigidity of compound **3**, demonstrated by VT NMR spectroscopy, implies a low energy difference between the *nido*- and *closo*-isomers and a low free energy barrier for the isomerisation process. DFT-calculations show that the optimized *nido*-structure of **3** is 6.6 kcal/mol lower in energy than that of the *closo*-isomer (Figure 4). Although small, this difference is larger than the 2.5 kcal/mol calculated for the cationic *nido* and *closo* isomers [(PMe₃)(PPh₃)(NC₅H₅)RhSB₉H₉]⁺.¹¹ This result is in agreement with the NMR spectroscopic data which revealed that the *closo*-isomer is the only species detected in solution for this *bis*-PR₃-ligated 11-vertex polyhedral cation.

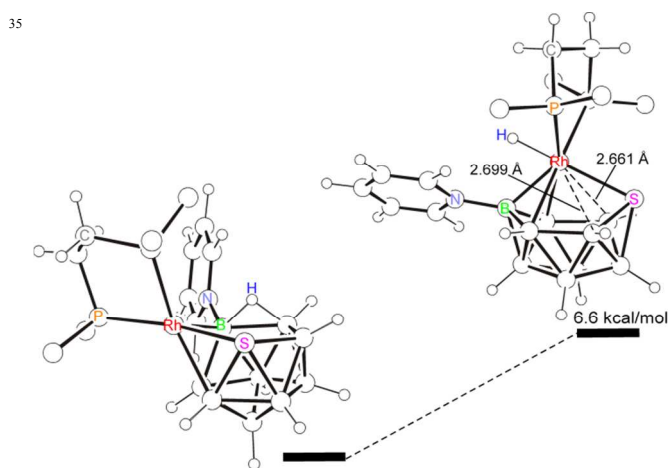


Fig. 4 DFT-calculated energies and structures, computed at the B3LYP/6-31G*/LANL2DZ level for the *nido*- and *closo*-isomers of **3**.

Regarding the free energy value of the *nido* / *closo* tautomerization, for simplicity, the dynamic process has been treated as an equally populated two-sites exchange involving the two doublets marked with red triangles in Figure 3. This treatment has provided a free energy, ΔG_{213}^\ddagger , of 8.6 kcal/mol (see ESI for more details).

This rapid interconversion between tautomers is clearly reminiscent of the fluxional behavior that exhibits eleven-vertex *nido*-metallaheteroboranes based on the *nido*-[MEB₉H₁₀] unit, where M = Rh, E = NH or S; and M = Pt, E = CH.^{18, 19, 21} Thus, the fluxional behaviour of these species is similarly owned to a rapid internal “switching” and half-rotation of the metal centre across the formal {EB₉H₁₀} ‘mirror plane’. The transition state for this fluxional process, calculated for [8,8-(PH₃)₂-*nido*-8,7-RhEB₉H₁₀], where E is NH or S,¹⁸ features a Rh(1)–H–B(3) bridging bond in a C_s *closo*-type eleven-vertex geometry that resembles the structure proposed for the *closo*-isomer of compound **3**.

Table 2 Free energy values for the rearrangement processes involved in eleven-vertex metallaheteroboranes

Compound	ΔG^\ddagger (kcal/mol)	Reference
[(PPh ₃) ₂ RhSB ₉ H ₁₀]	14	19
[(PPh ₂ Me) ₂ RhSB ₉ H ₁₀]	12	6
[(dppp)RhSB ₉ H ₁₀]	13	22
[(dppp)RhSB ₉ H ₉ (OEt)]	>15	22
[(dppe)RhSB ₉ H ₁₀]	11 ^a	this work
[(dppe)RhSB ₉ H ₉ (NC ₅ H ₅)] ⁺ (3)	9	this work
[(PPh ₃) ₂ RhNB ₉ H ₁₁]	11	18
[(PMe ₂ Ph) ₂ PtCB ₉ H ₁₁]	15	21
[(PMe ₂ Ph) ₂ PtCB ₉ H ₁₀ (OEt)]	>18	18

^aThis cluster was reported in refs ¹⁶ and ²² but its fluxional behaviour is reported here for the first time (see ESI).

Table 2 lists the free energy values for the rearrangement processes involved in neutral eleven-vertex metallaheteroboranes of general formulation, [8,8-(L)₂-*nido*-8,7-MEB₉H₁₀], where M = Rh, E = NH or S; M = Pt, E = CH; and (L)₂ = monodentate or bidentate phosphine ligands, together with the energy measured in this work for the cationic species **3**. The data reveal that **3** exhibits a lower energy barrier than the neutral species,

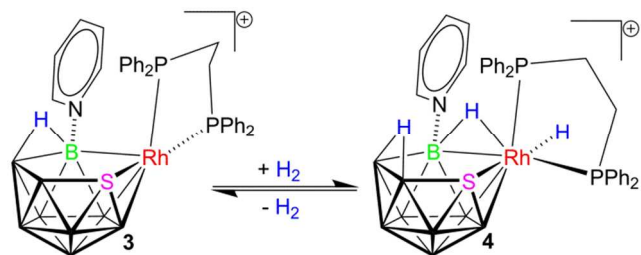
demonstrating that the ligation of the thiaborane moiety to the metal centre is more labile.

Reactivity with dihydrogen. The activation of dihydrogen by polyhedral boron containing-compounds is rare. Thus, there are few examples of metallaheteroboranes that react with H₂ to give the addition products as the result of the heterolytic splitting of the H–H bond on the clusters.^{8, 12, 13, 23} The red, air stable rhodium complex, **2**, does not react in an atmosphere of 10 bar of dihydrogen. In contrast, the orange-red cationic species, **3**, reacts instantaneously with H₂ to give a pale yellow solution. The study of this reaction system by multielement NMR spectroscopy has allowed the characterization of two new cationic hydridorhodathiaboranes.

The ¹H–{¹¹B} NMR spectrum of the reaction mixture shows a *pseudo*-quintet and *pseudo*-quartet at δ(¹H) –10.83 and –11.32 in a 0.7:1 relative intensity ratio, respectively. These two resonances can be safely assigned to Rh–H hydride ligands of two complexes. Between –5 and –7 ppm, the ¹H–{¹¹B} NMR spectrum displays a *pseudo*-triplet and a doublet of doublets also in a 0.7:1 intensity ratio. These signals broaden significantly, losing the coupling constants, when the broad-band boron decoupler is turned off. Therefore, these resonances can be assigned to hydrogen atoms that occupy bridging positions along the Rh(8)–B(9) edge of two eleven-vertex *nido*-clusters. In the negative region of the spectrum there are also two broad peaks at –3.39 and –4.06 ppm with a 1:0.7 relative intensity ratio, respectively. These resonances broaden in the ¹H NMR spectrum, being diagnostic of the presence of B–H–B bridging hydrogen atoms in the deltahedral clusters (the ¹H, ¹¹B, and ³¹P spectra are depicted in Figures S1, ESI).

The ³¹P–{¹H} NMR spectrum of this reaction mixture is also quite informative. At 223 K, there are four doublets of doublets between δ(³¹P) +75 and +60 in a 1:1:0.7:0.7 relative intensity ratio. These ³¹P resonances correspond to the chelating phosphine ligands of two clusters that contain the {RhH(dppe)} fragment as structural constituent. [¹H–³¹P]-HMBC experiments allowed the correlation of the proton resonances of the hydrides ligands with the dppe ligands to which they are associated at the rhodium centre. The assignment agrees with the correlation that is inferred from the analysis of the relative intensities found in the ¹H and ³¹P NMR spectra.

According to these NMR data, we propose that the reaction between **3** and H₂ affords a mixture of two hydridorhodathiaborane isomers of formulation, [8,8,8-(H)(η⁴-dppe)-μ-8,9-(H)-9-(NC₅H₅)-*nido*-8,7-RhSB₉H₉]⁺ (**4**).



Scheme 3 Reversible reaction of **3** with H₂. For clarity, only one isomer for **4** is depicted (*vide infra*).

Interestingly, the ³¹P–{¹H} NMR spectrum of the isomeric mixture, **4**, under a 10 bar atmosphere of H₂ at 300 K (Fig. S4)

shows a doublet at +54.6 ppm that corresponds to the cationic parent complex, **3**. In addition, the release of dihydrogen in the quick valve pressure NMR tube results in a significant increase of **3**. These observations allow us to conclude that the mixture of hydridorhodathiaboranes, **4**, and the reactant, **3**, are in equilibrium. To our knowledge, this cationic system together with the previously reported carbene-ligated pair, [1,1-(Ime)(PPh₃)-3-(NC₅H₅)-*closo*-1,2-RhSB₉H₈] and [8,8,8-(H)(Ime)(PPh₃)-9-(NC₅H₅)-*nido*-8,7-RhSB₉H₉], where Ime = 1,3-dimethylimidazol-2-ylidene, represent the only cases of chemical equilibria between polyhedral boron-based clusters sustained by the reversible splitting of H₂.

DFT-calculations revealed that the tautomers with the hydrogen atoms along the B(10)–B(11) and Rh(8)–B(9) edges afforded stable local energy minima, whereas the structures with bridging hydrogen atoms along the B(9)–B(10) or S(7)–B(11) were not stable. Thus, the two isomers, characterized by multielement NMR spectroscopy, are attributed to the different tetrahapto ligation of the thiaborane moiety to rhodium. There are three limiting configurations that can describe the {Rh(H)(dppe)}-to-η⁴-SB₉H₁₀(NC₅H₅) linkage, which were optimized by DFT-calculations and they are depicted in Figure 5.

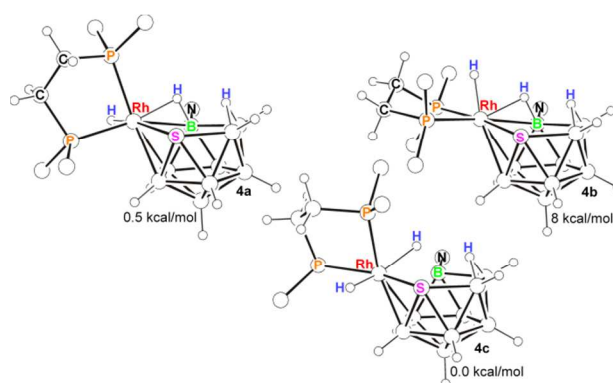


Fig. 5 Energy comparisons for DFT optimized metal-to-thiaborane configurational isomers of **4**

The three calculated isomers exhibit low energy differences, being the highest energy isomer that with the hydride ligand trans to the B(3)–B(4) edge, **4b**. In a similar fashion to the metallacarboranes, we have found that the *exo*-polyhedral configuration at the metal centre in hydridorhodathiaboranes is directed by the sulphur atom, which drives the hydride ligand *trans* to the position of this heteroatom. Based on these observations, we expected to find in **4** this ligand orientation as the most stable {Rh(H)(dppe)}-to-ηⁿ-SB₉H₁₀(NC₅H₅) configuration. It was surprising, therefore, to find that the optimization of the isomer with the hydride ligand trans to the B(9) vertex afforded a cluster, **4c**, with an energy that lies 0.5 kcal/mol lower than the isomer, **4a**, with the hydride trans to the sulphur vertex (Fig. 5). However, this cluster exhibits a long Rh(8)–B(9) distance at 2.773 Å (*versus* 2.478 Å and 2.410 Å in the isomers **4a** and **4b**, Fig. 5) that is clearly non-bonding. The resulting DFT-calculated isomer **4c** features a trihapto ligation of the {SB₉H₉(NC₅H₅)} moiety to a {Rh(H)₂(dppe)} group with two hydride ligands trans to each other. This DFT-calculated configuration is expected to result in a very large ²J_{HH} coupling

constant involving the hydrides, which is not observed experimentally. In conclusion, given the small energy differences between the three calculated structures, it is reasonable to assign the clusters **4a** and **4b** in Fig. 5 as the isomers detected by NMR.

A clockwise {Rh(H)(dppe)}-to- η^4 -{SB₉H₉(NC₅H₅)} rotation of $\sim 90^\circ$ in **4a** results in the formation of **4a**. In the isomer **4b**, the facial disposition of the Rh(8)–H hydride ligand, and the Rh(8)–H–B(9) and B(10)–H–B(11) hydrogen atoms may facilitate the reversible release of H₂, perhaps, through the formation of a Rh–(η^2 -H₂) dihydrogen intermediate that would be comparable to the side-on bonded dihydrogen complex, [8,8,8-(η^2 -H₂)(Ime)(PPh₃)-9-(NC₅H₅)-*nido*-8,7-RhSB₉H₈], calculated by DFT.¹²

Experimental section

General considerations

All reactions were carried out under an argon atmosphere using standard Schlenk-line techniques. Solvents were obtained from an Innovative Technology Solvent Purification System. [8,8,8-(H)(PPh₃)₂-9-(NC₅H₅)-*nido*-8,7-RhSB₉H₉] (**1**), was prepared according to the literature method.^{8, 9} Commercially available 1,2-bis(diphenylphosphino)ethane (dppe) was used as received without further purification. Preparative thin-layer chromatography (TLC) was carried out using 1 mm layers of silica gel G (Fluka, type GF254) made from water slurries on glass plates of dimensions 20 × 20 cm and dried in air at 25 °C. Infrared spectra were recorded on a Perkin-Elmer Spectrum 100 spectrometer, using an Universal ATR Sampling Accessory. NMR spectra were recorded on Bruker Avance 300-MHz and AV 400-MHz spectrometers, using ¹¹B, ¹¹B-¹H, ¹H, ¹H-¹¹B, ¹H{¹¹B(selective)} and ³¹P-¹H techniques. ¹H chemical shifts were measured relative to partially deuterated solvent peaks but are reported in ppm relative to tetramethylsilane. ¹¹B chemical shifts were measured relative to [BF₃(OEt)₂]. ³¹P (121.48 MHz) chemical shifts were measured relative to H₃PO₄ (85%). Mass spectrometric data were recorded on a MICROFLEX instrument operating in either positive or negative modes, using matrix-assisted laser desorption/ionization (MALDI). A nitrogen laser of 337 nm (photon energy of 3.68 eV) was used for the ionization processes, and the molecules under study were protected with a matrix of *trans*-2-[3-(4-*tert*-Butylphenyl)-2-methyl-2-propenylidene]malononitrile (DCTB). In each case there was an excellent correspondence between the calculated and measured isotopomer envelopes. A well-matched isotope pattern may be taken as a good criterion of identity.

X-ray structural analysis for compounds **2** and **3**

Crystals were grown by slow diffusion of hexane into a dichloromethane solution of the corresponding rhodathiaboranes, **2** and **3**. A suitable crystal of each cluster was coated with perfluoropolyether, mounted on a glass fiber and fixed in a cold nitrogen stream ($T = 100(2)$ K) to the goniometry head. In the case of **3**, several crystals were scrutinized to optimize size (intensity) and twin nature; eventually a not very intense slightly twinned crystal was selected as the best compromise for data collection. Data collection were performed on a Bruker Kappa APEX DUO CCD area detector diffractometer with monochromatic radiation $\lambda(\text{MoK}\alpha) = 0.7107073$ Å, using narrow frames (0.3° in ω). Intensities were integrated including Lorentz

and polarization effects with the SAINT-Plus program²⁴ and corrected for absorption effects by multiscan methods (SADABS).²⁵ The structures were solved using the SHELXS-97 program,²⁶ and refined against all F^2 data by full-matrix least-squares techniques (SHELXL-97).²⁷ Both structures were refined first with isotropic and later with anisotropic displacement parameters for non-disordered non-H atoms. Specific relevant details on each structure are described below. CCDC 1043935 and 1044383 contain the supplementary crystallographic data for this paper. These data can be obtained free of charge from the Cambridge Crystallographic Data Centre via www.ccdc.cam.ac.uk/data_request/cif.

Crystal data for **2**: C₃₁H₃₇B₉NP₂RhS•2(CH₂Cl₂); $M = 887.67$; red prism $0.238 \times 0.157 \times 0.102$ mm³; triclinic; $P-1$; $a = 9.8610(10)$, $b = 10.3668(10)$, $c = 19.485(2)$ Å, $\alpha = 93.404(2)^\circ$, $\beta = 91.461(2)^\circ$, $\gamma = 100.0580(10)^\circ$; $Z = 2$; $V = 1956.5(3)$ Å³; $D_c = 1.507$ g cm⁻³; $\mu = 0.873$ mm⁻¹; min. and max. absorption correction factors 0.809 and 0.898; $2\theta_{\text{max}} = 59.16^\circ$; 34075 reflections collected, 10118 unique ($R_{\text{int}} = 0.033$); number of data/restraints/parameters 10118/0/608; final GOF 1.044; $R_1 = 0.0303$ (8620 reflections, $I > 2\sigma(I)$); $wR(F^2) = 0.0731$ for all data. Hydrogen atoms have been observed in Fourier difference maps and freely refined, except H60A and H60B, in the dichloromethane molecule which were included from observed positions and refined with displacement riding parameters.

Crystal data for **3**: C₃₁H₃₈B₉NP₂RhS⁺ CF₃O₃S⁻ · CHF₃O₃S · CH₂Cl₂; $M = 1102.90$; orange block $0.271 \times 0.164 \times 0.074$ mm³; monoclinic; $C2/c$; $a = 11.2683(15)$, $b = 20.906(3)$, $c = 39.689(5)$ Å, $\beta = 91.817(2)^\circ$; $Z = 8$; $V = 9345(2)$ Å³; $D_c = 1.568$ g cm⁻³; $\mu = 0.750$ mm⁻¹; min. and max. absorption correction factors 0.744 and 0.916; $2\theta_{\text{max}} = 52.74^\circ$; 42710 reflections collected, 9525 unique ($R_{\text{int}} = 0.1109$); number of data/restraints/parameters 9525/24/587; final GOF 1.272; $R_1 = 0.1114$ (7443 reflections, $I > 2\sigma(I)$); $wR(F^2) = 0.2554$ for all data. All organic terminal hydrogens were included in calculated positions and refined with a usual riding strategy; the bridging hydrogen of the metallaborane, and those of the triflic acid and of the solvent molecule were not included in the model. Static disorder was observed both for a CF₃SO₃ moiety –refined with some geometrical restrictions– and for a solvent highly-disordered dichloromethane molecule.

Calculations

Calculations were performed using the Gaussian 09 package.²⁸ Structures were initially optimized using standard methods with the STO-3G* basis-sets for C, B, P, S, and H with the LANL2DZ basis-set for the metal atom. The final optimizations, including frequency analyses to confirm the true minima were performed using B3LYP methodology, with the 6-31G* and LANL2DZ basis-sets.

[1,1-(η^2 -dppe)-3-(NC₅H₅)-*closo*-1,2-RhSB₉H₈] (**2**)

108.0 mg (0.128 mmol) of [8,8,8-(H)(PPh₃)₂-9-(NC₅H₅)-*nido*-8,7-RhSB₉H₉] (**1**) was dissolved in 10 mL of CH₂Cl₂ in a Schlenk tube under an atmosphere of argon. Next, 50.8 mg (0.128 mmol) of dppe was added, and the reaction mixture was stirred at 55 °C for 16 h. The resulting orange solution was concentrated under vacuum, and applied to preparative TLC plates. Elution with 9:1 CH₂Cl₂/hexane gave an orange band ($R_f = 0.32$), from which an orange product was isolated, washing the silica-gel with pure dichloromethane. The product was characterized as **2**; after

crystallization from CH₂Cl₂/hexane, we isolated 48 mg (55% yield). ¹¹B-¹H} (128 MHz) and ¹H-¹¹B} NMR (300 MHz) in CD₂Cl₂ at 300 K {cluster resonances ordered as: assignment δ(¹¹B)/ppm [δ(¹H)/ppm for directly attached exo-hydrogen]}: B(3) +53.2 (B-NC₅H₅), BH(9) +26.6 [+3.98], 2BH(4,5) -1.1 [+2.09], BH(8) -12.5 [+2.59], 2BH(6,7) -24.2 [-0.14], 2BH(10,11) -32.9 [-0.21]. Additional ¹H NMR data are: δ = +7.89 (m, 4H; H_o-NC₅H₅ + C₆H₅), +7.73 (m, 4H; C₆H₅), +7.37 (m, 7H; H_o-NC₅H₅ + C₆H₅), +7.28 (t, ³J_{HH} = 8.0 Hz, 4H; C₆H₅), +7.14 (t, ³J_{HH} = 8.0 Hz, 2H; H_m-NC₅H₅), +7.08 (m, 4H; C₆H₅), +2.45 (m, 2H; CH₂), +2.05 (m, 2H; CH₂). ³¹P-¹H} NMR (162 MHz, CD₂Cl₂, 298 K): δ = +64.7 (d, ¹J_{RhP} = 150 Hz). Anal. Calcd. for C₃₁H₃₇B₉NP₂RhS: C, 51.87; H, 5.19; N, 1.95; S, 4.45. Found: C, 50.75; H, 5.03; N, 2.06; S 4.63. LRMS (MALDI/DCTB): *m/z*: calcd for C₃₁H₃₅B₉NP₂RhS: 716.7 [M-(3H)]⁺; found 716.2. Isotope envelopes match those calculated from the known isotopic abundances of the constituent elements.

[8,8-(*η*²-dppe)-9-(NC₅H₅)-nido-8,7-RhSB₉H₉][OTf] (3)

32.3 mg (0.045 mmol) of [1,1-(*η*²-dppe)-3-(NC₅H₅)-*closo*-1,2-RhSB₉H₈] (2) was dissolved in 5 mL of CH₂Cl₂ in a Schlenk tube under an atmosphere of argon. The resulting orange suspension was treated with 6.76 mg (0.045 mmol) of triflic acid (TfOH), and the reaction mixture was stirred at room temperature for 30 minutes. The solvent was reduced under vacuum until an approximate volume of 0.5 mL. Addition of hexane gave an orange precipitate that was washed with hexane (3 x 3 mL). The solid was dried under vacuum, and it was characterized as compound 3. The compound was crystallized from CH₂Cl₂/hexane to give 38 mg (96% yield). ¹¹B-¹H} (128 MHz) and ¹H-¹¹B} NMR (300 MHz) in CD₂Cl₂ at 300 K {cluster resonances ordered as: assignment δ(¹¹B)/ppm [δ(¹H)/ppm for directly attached exo-hydrogen]}: B(9) +38.2 (B-NC₅H₅), BH +15.1 [+3.75], 2BH +11.6 [+3.19], 5BH -17.2 [1H +2.10, 2H +1.61, 2H +1.26]. Additional ¹H-¹¹B} NMR data are: δ = +8.25 (t, ³J_{HH} = 8.0 Hz, 1H; H_p-NC₅H₅), +7.61 to +7.39 (m, 24H; H_o-NC₅H₅, H_m-NC₅H₅, C₆H₅), +2.95 (m, 2H; CH₂), -3.35 (s, 1H; BHB). ³¹P-¹H} NMR (162 MHz, CD₂Cl₂, 300 K): δ = +54.6 (d, ¹J_{RhP} = 118 Hz). ³¹P-¹H} NMR (162 MHz, CD₂Cl₂, 183 K): δ = *ca.* +58.0 (this resonance overlays with the next doublet), +57.4 (br. d, ¹J_{RhP} = 141 Hz), +46.3 (br. d, ¹J_{RhP} = 123 Hz). Anal. Calcd. for C₃₂H₃₈B₉F₃NO₃P₂RhS₂: C, 44.28; H, 4.41; N, 1.61; S, 7.39. Found: C, 42.81; H, 4.32; N, 1.69; S 7.52. LRMS (MALDI/DCTB): *m/z*: calcd for C₃₁H₃₄B₉NP₂RhS: 715.7 [M-(4H)]⁺; found 715.2. Isotope envelopes match those calculated from the known isotopic abundances of the constituent elements.

Reaction of [8,8-(*η*²-dppe)-9-(NC₅H₅)-nido-8,7-RhSB₉H₉][OTf] (3) with H₂

In a quick pressure valve NMR tube, 3 mg (0.015 mmol) of 3 was dissolved in 0.3 mL of CD₂Cl₂. The tube was evacuated under vacuum at the temperature of liquid nitrogen, and subsequently, exposed to 10 bar of hydrogen. The resulting sample was studied by NMR spectroscopy. The data were consistent with the presence in a 1:0.7 ratio of two cationic hydridorhodathiaboranes of formulation, [8,8-(*η*²-dppe)(H)-9-(NC₅H₅)-nido-8,7-RhSB₉H₁₀]⁺. The isomers were not separated and the NMR data below correspond to samples that contain both species. NMR ¹¹B-¹H} (128 MHz; CD₂Cl₂; 298 K): δ = +16.6, +11.1, +4.8,

+3.7, -8.8, -12.1, -13.1, -15.9, -17.1, -19.8, -23.4, -24.8. The signals are broad and indistinguishable for both isomers. NMR ¹H-¹¹B} (400 MHz, CD₂Cl₂, 290 K): δ = +8.60 (d, ³J_{HH} = 6.0 Hz, 2H; H_o-NC₅H₅), +8.21 (t, ³J_{HH} = 7.6 Hz, 1H; H_p-NC₅H₅), +8.00 (t, ³J_{HH} = 8.0 Hz, 1H; H_p-NC₅H₅), +7.92 to +6.81 (m, 40H; C₆H₅ + NC₅H₅), +4.01 (s, 1H; BH), +3.80 (s, 0.7H; BH), +3.58 (s, 1H; BH), +3.27 (m, 1H; CH₂), +2.98 (m, 2H; CH₂), +2.89 (s, 1H; BH), +2.79 (m, 2H, CH₂), +2.61 (m, 2H, CH₂), +2.41 (s, 3H; BH), +2.35 (m, 0.7H; CH₂), +1.83 (s, 1H; BH), +1.75 (s, 0.7B; BH), +1.67 (s, 1B; BH), +1.35 (s, 1B; BH), -3.39 (s, 1H; BHB), -4.06 (s, 0.7H; BHB), -5.79 (*pseudo* t, 0.65H, ¹J_{RhH} + ²J_{PH} = 15 Hz, BHRh), -6.72 (dd, ¹J_{RhH} = 55 Hz, ²J_{PH} = 16 Hz, 1H; BHRh), -10.83 (*pseudo* quintet, ¹J_{HRh} + ²J_{HP} + ²J_{HH} = 14.0 Hz, 0.7H; RhH), -11.32 (*pseudo* quartet, ¹J_{HRh} + ²J_{HP} ≈ 23 Hz; 1H; RhH). NMR ³¹P-¹H} (162 MHz; CD₂Cl₂; 223 K): δ = +72.9 (br. dd, ¹J_{RhP} = 117 Hz, ²J_{PP} = 19 Hz, 1P_A; isomer A), +67.4 (dd, ¹J_{RhP} = 93 Hz, ²J_{PP} = 17 Hz, 1P_A; isomer A), +65.4 (dd, ¹J_{RhP} = 133 Hz, ²J_{PP} = 9 Hz, 0.7P_B; isomer B), +61.3 (br dd, ¹J_{RhP} = 97 Hz, ²J_{PP} = 9 Hz, 0.7P_B; isomer B). [¹H-³¹P]-HMBC (400 MHz, CD₂Cl₂, 193 K) {ordered as (δ_H, δ_P) correlation}: (-11.32, +73.6), (+3.09, +73.6), (+2.55, +73.6), (-11.32, +67.9), (+2.34, +67.9), (-10.83, +65.7), (+3.39, +61.8), (+2.94, +61.8), (+2.15, +61.8); all the ³¹P resonances exhibit correlations with aromatic signals.

Conclusions

The hydridorhodathiaborane, 1, reacts with the bidentate phosphine, dppe, to give the chelate, 2, as product of PPh₃ substitution at the metal centre and cluster dehydrogenation. This simple synthetic procedure can be *a priori* extended to other bidentate phosphine ligands, being a potential convenient way of tuning the reactivity of these 11-vertex rhodathiaboranes by the modification of the composition of the ligands at the metal centre. It has been already demonstrated that the change of the metal-bound ligands in pyridine-ligated 11-vertex rhodathiaboranes [1,1-(PR₃)₂-3-(NC₅H₅)-*closo*-1,2-RhSB₉H₈] has large consequences in their reactivity with strong Brønsted acids.^{11, 13, 14}

In this regard, the *bis*-PPh₃-ligated *closo*-derivative reacts with TfOH to afford an equilibrium that involves the cationic species [1,1-(PPh₃)₂-*μ*-1,3-(H)-3-(NC₅H₅)-*closo*-1,2-RhSB₉H₈]⁺, and neutral OTf-ligated compound [8,8-(TfO)(PPh₃)-3-(NC₅H₅)-nido-8,7-RhSB₉H₉] and [HPPH₃]⁺, which is formed upon protonation of the released PPh₃ ligand.¹³ The introduction of more basic phosphines such as PMe₃ and PMe₂Ph hinders the dissociation of the ligands upon protonation of the cage, stabilizing the cationic clusters, [1,1-(PPh₃)₂-*μ*-1,3-(H)-3-(NC₅H₅)-*closo*-1,2-RhSB₉H₈]⁺. Interestingly, a crystal of the *bis*-PPh₃PMe₃-ligated cation was found to contain three different isomers in the unit cell, one with featuring an 11-vertex *nido*-structure.¹¹ This uncommon case of conformational isomerism implies a labilization of the ligation between the pyridine-substituted thiaborane moiety and the rhodium center, which is promoted by protonation. In solution, however, these cationic clusters do not exhibit dynamic processes that could involve stereochemical non-rigid molecules

The new work reported herein demonstrates that the chelating phosphine, dppe, induces a higher level of non-rigidity, leading to the formation of a prototropic *closo*↔*nido* equilibrium in

solution. This tautomerization involves a proton shift between bridging positions along the Rh(1)–B(3) and the B(9)–B(10) edges of the *closo*- and *nido*-tautomers, respectively.

This interconversion between tautomers is performed through hapticity changes in the ligation between the pyridine-substituted thiaborane moiety and the rhodium centre. This dynamic process together with the enhancement of the Lewis acidity that occurs upon protonation of the cluster facilitate the interaction of the dihydrogen molecule with the cationic rhodathiaborane, **2**, leading to the efficient heterolytic splitting of the H–H bond and the subsequent formation of the hydridorhodathiaboranes, **4a** and **4b**. A further illustration of the different reactivity induced by the phosphine ligands is the fact that the mixture of isomers, **4a** and **4b**, is unstable in the absence of an atmosphere of H₂, regenerating the parent cation, **2**, by release of dihydrogen. This contrasts with the *bis*-PR₃-ligated analogues, [8,8,8-(H)(PR₃)₂-9-(NC₅H₅)-*nido*-8,7-RhSB₉H₁₀]⁺, where PR₃ = PPh₃, PPh₃ and PMe₃, or, PPh₃ and PMe₂Ph, which are stable in the absence of free H₂.^{8, 29}

Insisting in the introductory paragraph, the possibility to modify the chemical and structural basis of this class of 11-vertex rhodathiaboranes is without doubt a driving force behind the study of the reaction chemistry of these polyhedral clusters. In this regard, the protonation of metallaheteroboranes to enhance their stereochemical non-rigidity and their Lewis acidity is a simple method that, in principle, could be of general application in polyhedral boron-containing compounds. And the results reported herein and in previous works augur well for the tailoring of new metallaheteroboranes that may be useful in, for example, solving problems in catalysis.

Notes and references

^a Instituto de Síntesis Química y Catálisis Homogénea (ISQCH), Universidad de Zaragoza-Consejo Superior de Investigaciones Científicas, 50009-Zaragoza, Spain.. Tel: 34 976 761143; E-mail: oro@unizar.es, rmacias@unizar.es

^b Center of Research Excellence in Petroleum Refining and Petrochemicals, King Fahd University of Petroleum and Minerals (KFUPM), Dhahran 31261, Saudi Arabia

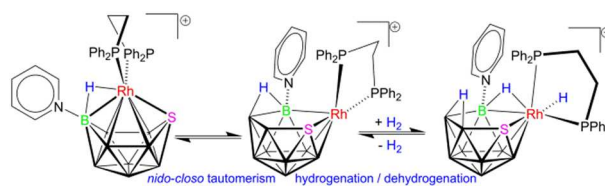
† Dedicated to the memory of Professor Ken Wade, a “pattern-maker” in cluster chemistry.

‡ Electronic Supplementary Information (ESI) available: Additional NMR data for compounds **2**, **3**, **4** and the previously reported [(dppf)RhSB₉H₁₀]. See DOI: 10.1039/b000000x/.

1. *Applied Homogeneous Catalysis with Organometallic Compounds*, Wiley-VCH Verlag GmbH, 2008.
2. J. D. Kennedy, in *Prog. Inorg. Chem.*, John Wiley & Sons, Inc., 2007, pp. 519-679; J. D. Kennedy, in *Prog. Inorg. Chem.*, John Wiley & Sons, Inc., 2007, pp. 211-434; L. Barton, Strivastava, D. K., in *Comprehensive Organometallic Chemistry II*, ed. E. W. Abel, Stone, F. G. A., Wilkinson, G., Pergamon, New York, 1995, vol. 1, pp. 275-372; A. S. Weller, in *Comprehensive Organometallic Chemistry III*, eds. R. H. Crabtree and D. M. P. Mingos, Elsevier, Oxford, 2007, vol. 3, pp. 133-174; R. N. Grimes, in *Comprehensive Organometallic Chemistry*, eds. G. Wilkinson, F. G. A. Stone and E. W. Abel, Pergamon Press Ltd., Oxford, 1982, vol. 1, ch. 5.5, pp. 459-542; R. N. Grimes, in *Comprehensive Organometallic Chemistry II*, eds. E. W. Abel, F. G. A. Stone and G. Wilkinson, Pergamon, Oxford, 1995, vol. 1, pp. 373-430; L. Wesemann, in *Comprehensive Organometallic Chemistry*, eds. D. M. P. Mingos and R. H. Crabtree, Elsevier, Oxford, 2007, vol. 3, pp. 113-131; N. S. Hosmane and J. A. Maguire, in *Comprehensive Organometallic Chemistry III*, ed. D. M. P. M. H. Crabtree, Elsevier, Oxford, 2007, pp. 175-264.

3. A. Alvarez, R. Macias, M. J. Fabra, M. L. Martin, F. J. Lahoz and L. A. Oro, *Inorg. Chem.*, 2007, **46**, 6811-6826.
4. B. Calvo, R. Macias, M. J. Artigas, F. J. Lahoz and L. A. Oro, *Inorg. Chem.*, 2012, **52**, 211-221.
5. B. Calvo, Á. Álvarez, R. Macias, P. García-Orduña, F. J. Lahoz and L. A. Oro, *Organometallics*, 2012, **31**, 2986-2995.
6. B. Calvo, M. Kess, R. Macias, C. Cunchillos, F. J. Lahoz, J. D. Kennedy and L. A. Oro, *Dalton Trans.*, 2011, **40**, 6555-6564.
7. Á. Álvarez, R. Macias, J. Bould, C. Cunchillos, F. J. Lahoz and L. A. Oro, *Chem. Eur. J.*, 2009, **15**, 5428-5431.
8. Á. Álvarez, R. Macias, M. J. Fabra, F. J. Lahoz and L. A. Oro, *J. Am. Chem. Soc.*, 2008, **130**, 2148-2149.
9. Á. Álvarez, R. Macias, J. Bould, M. J. Fabra, F. J. Lahoz and L. A. Oro, *J. Am. Chem. Soc.*, 2008, **130**, 11455-11466.
10. B. Calvo, B. Roy, R. Macias, M. J. Artigas, F. J. Lahoz and L. A. Oro, *Inorg. Chem.*, 2014; B. Calvo, M. Keß, R. Macias, R. Sancho, F. J. Lahoz and L. A. Oro, *J. Coord. Chem.*, 2014, 1-12.
11. B. Calvo, R. Macias, M. J. Artigas, F. J. Lahoz and L. A. Oro, *Dalton Trans.*, 2014, **43**, 5121-5133.
12. B. Calvo, R. Macias, V. Polo, M. J. Artigas, F. J. Lahoz and L. A. Oro, *Chem. Commun.*, 2013, **49**, 9863-9865.
13. B. Calvo, R. Macias, M. J. Artigas, F. J. Lahoz and L. A. Oro, *Chem. Eur. J.*, 2013, **19**, 3905-3912.
14. B. Calvo, R. Macias, C. Cunchillos, F. J. Lahoz and L. A. Oro, *Organometallics*, 2012, **31**, 2526-2529.
15. K. Wade, *Adv. Inorg. Chem. Radiochem.*, 1976, **18**, 1-66.
16. K. J. Adams, T. D. McGrath, G. M. Rosair, A. S. Weller and A. J. Welch, *J. Organomet. Chem.*, 1998, **550**, 315-329.
17. D. G. Evans and D. M. P. Mingos, *J. Organomet. Chem.*, 1982, **240**, 321-327; J. D. Kennedy, *Main Group Met. Chem.*, 1989, **12**, 149-154; J. D. Kennedy, in *The Borane-Carborane-Carbocation Continuum*, ed. J. Casanova, Wiley, New York, 1998, pp. 85-116; J. Bould, S. J. Teat and J. D. Kennedy, *Collect. Czech Chem. Commun.*, 2007, **72**, 1631-1638; J. Bould, P. A. Cooke, U. Dorfler, J. D. Kennedy, L. Barton, N. P. Rath and M. Thornton-Pett, *Inorg. Chim. Acta*, 1999, **285**, 290-295.
18. R. Macias, J. Bould, J. Holub, J. D. Kennedy, B. Štibr and M. Thornton-Pett, *Dalton Trans.*, 2007, 2885 – 2897.
19. G. Ferguson, M. C. Jennings, A. J. Lough, S. Coughlan, T. R. Spalding, J. D. Kennedy, X. L. R. Fontaine and B. Štibr, *J. Chem. Soc., Chem. Commun.*, 1990, 891-894.
20. J. Bould and R. Macias, *J. Organomet. Chem.*, 2014, **761**, 120-122.
21. B. Štibr, T. Jelinek, J. D. Kennedy, X. L. R. Fontaine and M. Thornton-Pett, *J. Chem. Soc., Dalton Trans.*, 1993, 1261-1267.
22. R. Macias, N. P. Rath and L. Barton, *Organometallics*, 1999, **18**, 3637-3648.
23. Z. J. Yao, X. K. Huo and G. X. Jin, *Chem. Commun.*, 2012, **48**, 6714-6716.
24. Bruker, in *SAINT-PLUS (Version 6.01)*, ed. M. Bruker AXS Inc, WI, 2001.
25. G. M. Sheldrick, SADABS Program for Correction of Area Detector Data, University of Göttingen, Göttingen, Germany, 1999.
26. G. Sheldrick, *Acta Cryst.*, 1990, **A46**, 467-473.
27. G. M. Sheldrick, *Acta Cryst.*, 2008, **A64**, 112-122.
28. M. J. Frisch, G. W. Trucks, H. B. Schlegel, G. E. Scuseria, M. A. Robb, J. R. Cheeseman, J. A. M. Jr., T. Vreven, K. N. Kudin, J. C. Burant, J.M. Millam, S. S. Iyengar, J. Tomasi, V. Barone, B. Mennucci, M. Cossi, G. Scalmani, N. Rega, G. A. Petersson, H. Nakatsuji, M. Hada, M. Ehara, K. Toyota, R. Fukuda, J. Hasegawa, M. Ishida, T. Nakajima, Y. Honda, O. Kitao, H. Nakai, M. Klene, X. Li, J. E. Knox, H. P. Hratchian, J. B. Cross, V. Bakken, C. Adamo, J. Jaramillo, R. Gomperts, R. E. Stratmann, O. Yazyev, A. J. Austin, R. Cammi, C. Pomelli, J. Ochterski, P. Y. Ayala, K. Morokuma, G. A. Voth, P. Salvador, J. J. Dannenberg, V. G. Zakrzewski, S. Dapprich, A. D. Daniels, M. C. Strain, O. Farkas, D. K. Malick, A. D. Rabuck, K. Raghavachari, J. B. Foresman, J. V. Ortiz, Q. Cui, A. G. Baboul, S. Clifford, J. Cioslowski, B. B. Stefanov, G. Liu, A. Liashenko, P. Piskorz, I. Komaromi, R. L. Martin, D. J. Fox, T. Keith, M. A. Al-Laham, C. Y. Peng, A. Nanayakkara, M. Challacombe, P. M. W. Gill, B. G. Johnson, W. Chen, M. W. Wong, C. Gonzalez and J. A. Pople, Gaussian, Inc, Wallingford, CT, 2004.
29. Á. Álvarez, B. Calvo, R. Macias, F. J. Lahoz and L. A. Oro, *Organometallics*, 2014, **33**, 3137-3153.

Graphical and textual abstract for the Table of contents entry.



The $\{\text{SB}_9\text{H}_8(\text{NC}_5\text{H}_5)\}$ -to- $\{\text{Rh}(\text{dppe})\}$ linkage is labilized is upon protonation leading to a *closo* \leftrightarrow *nido* tautomerism; non-rigidity and higher Lewis acidity, induced by the proton, make possible the H_2 activation on the cationic rhodathiaboran